JCB Journal of Cell Biology

REPORT

Liquid–liquid phase separation mediates the formation of herpesvirus assembly compartments

Sheng Zhou[1,2], Zhifei Fu[2,3,4,5], Ziwei Zhang[1,2], Xing Jia[1,6], Guangjun Xu[1,2], Long Sun[1,2], Fei Sun[4,6,7], Pu Gao[1,4], Pingyong Xu[2,4,5], and Hongyu Deng[1,2,4]

Virus assembly, which takes place during the late stage of viral replication, is essential for virus propagation. However, the underlying mechanisms remain poorly understood, especially for viruses with complicated structures. Here, we use correlative light and electron microscopy to examine the formation of cytoplasmic virion assembly compartments (cVACs) during infection by a γ-herpesvirus. These cVACs are membraneless organelles with liquid-like properties. Formation of cVACs during virus infection is mediated by ORF52, an abundant tegument protein. ORF52 undergoes liquid–liquid phase separation (LLPS), which is promoted by both DNA and RNA. Disrupting ORF52 phase separation blocks cVACs formation and virion production. These results demonstrate that phase separation of ORF52 is critical for cVACs formation. Our work defines herpesvirus cVACs as membraneless compartments that are generated through a process of LLPS mediated by a tegument protein and adds to the cellular processes that are facilitated by phase separation.

Introduction

In order to efficiently fulfill their biological functions, cells must spatially organize and biochemically regulate numerous biological processes in the vast yet densely packed subcellular space. One way to increase reaction kinetics and efficiency and to achieve spatiotemporal control is to form compartments so as to concentrate reaction components together. Classic organelles, such as the ER or Golgi apparatus, are membrane-bound compartments and are essential in creating order for various cellular processes. A wealth of data published in recent years has shown that membraneless organelles, such as nucleoli and stress granules, are also critical in subcellular organization and play important roles in many distinct biological processes (Boeynaems et al., 2018; Mitrea and Kriwacki, 2016; Shin and Brangwynne, 2017). These membraneless organelles, or condensates, are mostly formed by liquid–liquid phase separation (LLPS), a process in which specific molecules are assembled into a liquid-like compartment that stably coexists with the surrounding liquid milieu (Banani et al., 2017; Shin and Brangwynne, 2017). The condensates thus formed usually contain DNA- or RNA-binding proteins with multivalent domains or intrinsically disordered regions (IDRs). Weak interactions between multivalent domains and additional interactions between nucleic acids and IDRs are the main driving forces underlying LLPS (Shin and Brangwynne, 2017). The liquid-like composition and lack of membranes allow these structures to remain in a dynamic equilibrium with their surroundings and rapidly reorganize in response to signals. Moreover, emerging evidence has shown that condensates and membrane-bound organelles interact in many biological processes including signal transduction and cargo sorting (Zhao and Zhang, 2020).

As intracellular parasites, viruses must modulate the environment of infected cells to facilitate processes which are crucial for their own propagation, including genome replication and virion assembly. Some viruses do this by establishing specialized subcellular structures, also known as viral factories. For instance, positive-strand RNA viruses such as hepatitis C virus, Zika virus, and coronaviruses, re-organize host membranes (mainly ER) to form double-membrane vesicles (DMVs) for viral genome replication (Cortese et al., 2017; Du Toit, 2020; Paul et al., 2014). Virion assembly, which takes place following viral genome replication, involves packaging of the viral genome and assembly of all the structural components into a mature viral particle. This is an essential yet complex step in the virus life cycle, particularly so for viruses with large genome sizes

[1]CAS Key Laboratory of Infection and Immunity, Institute of Biophysics, Chinese Academy of Sciences, Beijing, China; [2]University of Chinese Academy of Sciences, Beijing, China; [3]Public Technology Service Center, Fujian Medical University, Fujian, China; [4]CAS Center for Excellence in Biomacromolecules, Institute of Biophysics, Chinese Academy of Sciences, Beijing, China; [5]CAS Key Laboratory of RNA Biology, Institute of Biophysics, Chinese Academy of Sciences, Beijing, China; [6]Center for Biological Imaging, Institute of Biophysics, Chinese Academy of Sciences, Beijing, China; [7]National Laboratory of Biomacromolecules, Institute of Biophysics, Chinese Academy of Sciences, Beijing, China.

Correspondence to Hongyu Deng: hydeng@moon.ibp.ac.cn.

(i.e., large coding capacities for many structural proteins) and complicated virion structures such as herpesviruses.

Herpesviridae is a large family of DNA viruses that infect humans and other animals. Herpesviruses are divided into three subfamilies (α, β, and γ) based on their molecular organization, pathogenic outcomes, and clinical manifestations. A mature herpes virion contains, from the inside to the outside, double-stranded DNA genome, capsid, tegument, and envelope. Virus assembly takes place in the late stage of the virus life cycle. Capsids are assembled in the nucleus and package viral genomic DNA to form nucleocapsids. The nucleocapsids are then translocated into the cytoplasm, where they undergo tegumentation. This is a unique step in herpesvirus assembly, by which dozens of tegument proteins are recruited and assembled, through complicated interactions between capsid proteins and tegument proteins, and between different tegument proteins (Guo et al., 2010; Owen et al., 2015). Finally, the tegumented virus particles bud into host-derived vesicles for secondary envelopment and become mature virions which are competent for release (Peng et al., 2010). It has been reported that infection by HSV-1 (an α-herpesvirus) or HCMV (a β-herpesvirus) induces the formation of special compartments called cytoplasmic virion assembly compartments (cVACs) which recruit viral tegument proteins and host vesicles containing viral glycoproteins for virus assembly and maturation (Procter et al., 2018; White et al., 2020). During infection with murine gammaherpesvirus 68 (MHV-68, a γ-herpesvirus), cVAC-like structures were also observed under transmission electron microscopy (TEM), suggesting a conserved mechanism in herpesvirus assembly (Peng et al., 2010). Nevertheless, the detailed mechanisms underlying cVACs formation in herpesviruses remain poorly understood.

Tegument proteins, localized between the capsid and the envelope, are major components of herpes virions. During virus assembly, they serve as "linkages" between capsid and envelope and are indispensable for viral replication. We have previously identified a series of MHV-68 tegument proteins and investigated their roles in virion morphogenesis. In particular, we demonstrated that ORF33, ORF45, and ORF52 play essential roles in virus assembly (Bortz et al., 2007; Guo et al., 2009; Jia et al., 2016; Shen et al., 2015; Wang et al., 2012). Interestingly, in TEM or immunogold-staining images, areas of concentrated tegument proteins were often observed in the cytoplasm of infected cells (Guo et al., 2009; Jia et al., 2016; Peng et al., 2010). Nucleocapsids and vesicles containing enveloped virions were also frequently seen in these so-called "tegument deposit" areas, suggesting that these areas may serve as cVACs.

To investigate γ-herpesvirus cVACs formation in detail, we constructed a recombinant MHV-68 expressing a fluorescently tagged tegument protein, ORF52. With this recombinant virus, we investigated the formation and spatiotemporal change of cVACs in living cells. We found that cVACs have liquid organelle properties and ORF52 is required for cVACs formation. We also examined the conditions promoting ORF52 LLPS in vitro and in vivo. Finally, we demonstrated that the phase separation properties of ORF52 are critical for cVACs formation as well as virus assembly.

Results and discussion

cVACs are formed during γ-herpesvirus infection and have liquid properties

To investigate the formation of cVACs in MHV-68-infected cells in a temporal manner, we first constructed a recombinant MHV-68 expressing a fluorescently tagged tegument protein. We chose ORF52 because it is an abundant tegument protein (Bortz et al., 2003; Vidick et al., 2013) and our previous functional and structural analyses showed that it is essential for the cytoplasmic maturation of MHV-68 virions (Benach et al., 2007; Bortz et al., 2007; Wang et al., 2012). Briefly, the coding sequence for mCherry was inserted into the N-terminus of *ORF52* in the MHV-68 genome through a bacterial artificial chromosome (BAC) system, as described previously (Wu et al., 2011; Fig. S1, A and B). The recombinant BAC was transfected into 293T cells to produce MHV-68-mCherry-52 virus (Fig. S1, C and D). Because the lytic replication of herpesvirus is regulated in a cascade fashion and virus assembly takes place in the late stage of lytic replication, we infected cells with WT or MHV-68-mCherry-52 virus (MOI = 3) and followed viral infection by confocal microscopy from 8-h post infection (hpi). cVACs did not appear until 12 hpi in live-cell imaging, but started to accumulate in the cytoplasm as viral infection proceeded, with diameters ranging from 0.5 to 2 μm (Fig. 1 A and Video 1). The numbers and sizes of cVACs in cells infected with WT virus or recombinant virus are similar by image-based rendering and 3D analysis, indicating that tagging ORF52 with the fluorescent protein did not affect cVACs formation (Fig. S1, E and F).

To simultaneously investigate the ultrastructure of the cVACs we detected under fluorescence microscopy, we performed correlative light and electron microscopy (CLEM) with another recombinant virus named MHV-68-mEosEM-52 (Fig. S1, A–D). In this virus, ORF52 is tagged with mEosEM, a newly developed fluorescent protein that has been shown to survive Epon embedding and which works well in CLEM (Fu et al., 2020). We observed many nucleocapsids undergoing tegumentation and secondary envelopment in electron-dense compartments (Fig. 1 B). cVACs were localized close to but did not overlap with the TGN (Fig. S1 G). This is in agreement with previous observations that viral secondary envelopment process usually occurs near the TGN, which provides vesicles containing viral glycoproteins for virion maturation (Lv et al., 2019).

Because cVACs are utilized for viral tegumentation and secondary envelopment, these compartments should contain not only ORF52 but also other tegument proteins. Although tegument protein ORF33 is distributed in both the nucleus and the cytoplasm, and ORF52 is strictly cytoplasmic, ORF33 co-localized with ORF52 in cytoplasmic puncta. Similarly, tegument proteins ORF45 and ORF38 co-localized with ORF52 in cytoplasmic puncta. The co-localization of ORF33, ORF38, and ORF45 with ORF52 indicates that multiple tegument proteins are indeed concentrated in cVACs (Fig. 1, C and D). Taken together, these results demonstrate the formation of cVACs during γ-herpesvirus replication.

Results from live-cell imaging and CLEM showed that cVACs are membraneless structures and are somewhat spherical, which suggests that they may be formed by LLPS. To investigate

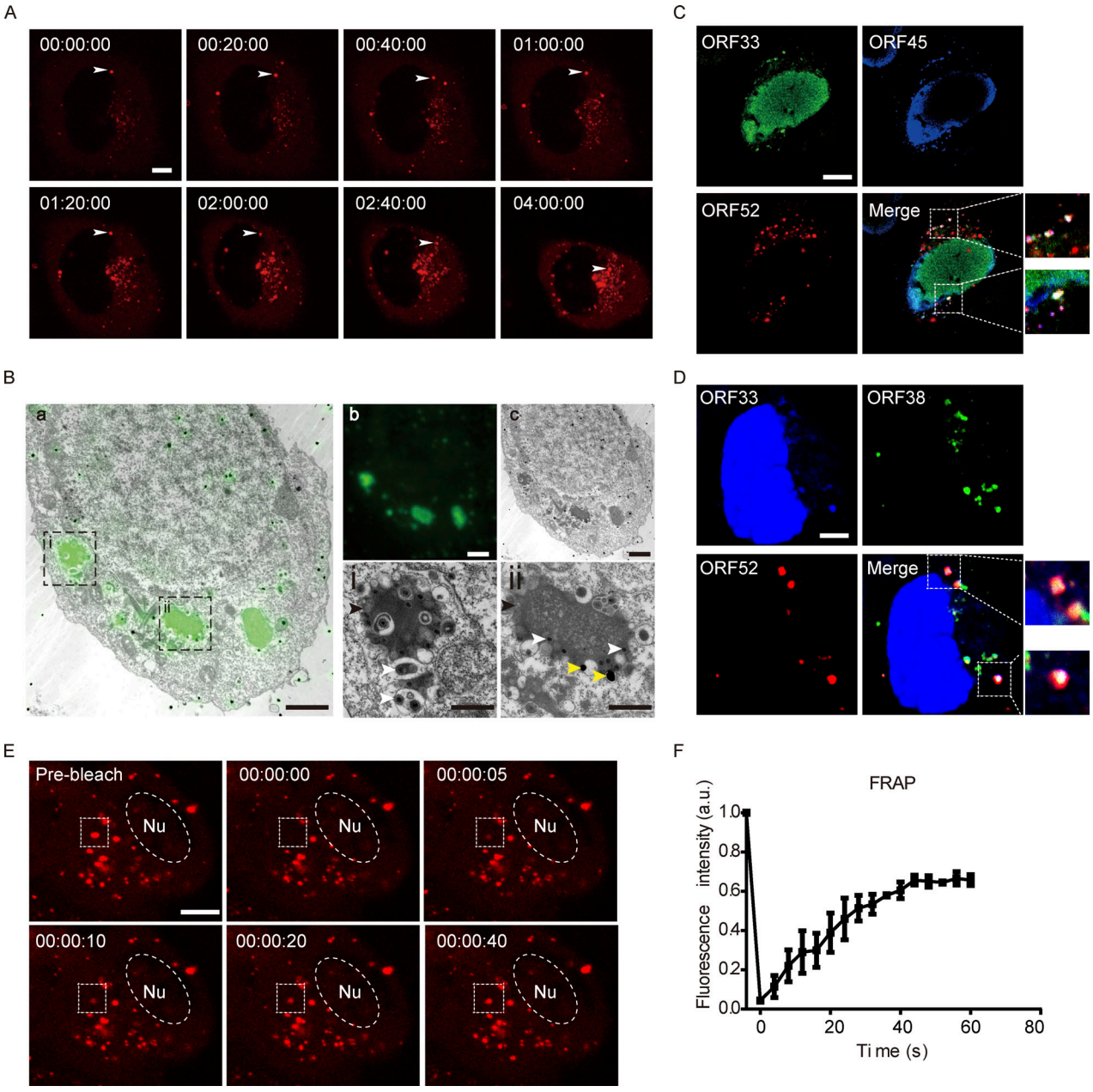

Figure 1. **cVACs are formed during γ-herpesvirus infection and have liquid properties. (A)** Time-lapse imaging of cVAC formation. COS-7 cells were infected with mCherry-ORF52 recombinant virus at a MOI of 3 and images were collected from 12 hpi (00:00:00). cVACs formed gradually in the cytoplasm over time. Bar: 5 µm. **(B)** CLEM images of a 100-nm ultrathin section of a cell infected by mEosEM-ORF52 recombinant virus. (a) Direct correlation between green fluorescence (representing ORF52) and TEM in a 293T cell. (b and c) Green fluorescence of cVACs in cytoplasm and TEM image of the whole 293T cell, respectively, after infection by recombinant virus. (i and ii) Enlarged images of the boxed areas in panel a, showing tegumentation and secondary envelopment of viral capsids in ORF52 puncta. Scale bars: 3 µm (main image); 1 µm (zoomed-in images). Black arrowhead: cVAC; white arrowheads: capsids; yellow arrowheads: gold nanoparticles used as fiducial markers for registration of light and electron microscopy images. **(C)** Co-localization of ORF33 (homologue of UL16 in HSV-1 and UL94 in HCMV) and ORF45 with cVACs. COS-7 cells were infected with mCherry-ORF52 virus (MOI = 3), and indirect immunofluorescence assay was performed at 24 hpi. ORF33 was detected using a mouse anti-ORF33 monoclonal antibody and ORF45 was detected using a rabbit anti-ORF45 polyclonal antibody. Secondary antibodies were conjugated with Alexa Fluor 488 (ORF33, green channel) or Alexa Fluor 647 (ORF45, blue channel). Bar: 5 µm. **(D)** Co-localization of ORF33 and ORF38 (homologue of UL11 in HSV-1 and UL99 in HCMV) with cVACs. The experiment was conducted as in C, except that ORF38 was detected using a rabbit anti-ORF38 polyclonal antibody. Bar: 5 µm. **(E)** FRAP of a cVAC in COS-7 cells at 37°C (box: bleach site; Nu, nucleus). These images are representative of at least three cells in which the cVAC puncta were photobleached. Bar: 5 µm. **(F)** Quantification of FRAP of cVAC puncta. Fluorescence intensities of cVACs were normalized to background and plotted over a 60-s time course. Shown are means ± SD. *n* = 3 cVAC puncta.

the liquid properties of cVACs, we performed fluorescence recovery after photobleaching (FRAP) experiments in COS-7 cells infected with the MHV-68-mCherry. At 18 hpi when cVACs had already formed in COS-7 cells, we photobleached a region of 2 μm diameter in a cVAC. The fluorescence signal recurred at just 10 s post-bleaching (Fig. 1 E and Video 2) and recovered nearly 60% within 1 min (Fig. 1 F), indicating that cVACs exhibit dynamic liquid properties. In addition, we treated infected COS-7 cells with 6% propylene glycol (PG) at 24 hpi. Time-lapse images showed that cVAC structures were disrupted by 6% PG treatment but reformed gradually after removing 6% PG from the cell-culture medium (Fig. S1 H), indicating that LLPS drives the formation of cVACs in infected cells.

ORF52 possesses LLPS properties and is required for cVACs formation

Membraneless organelles driven by LLPS usually contain proteins with the capacity to undergo phase separation. We hypothesized that formation of cVACs is driven by a viral tegument protein with the properties to induce LLPS. To identify which viral protein has this characteristic, we examined a series of tegument proteins for their distribution patterns in cells. Among these tegument proteins, only ORF52 formed spherical structures in vivo (Fig. S2 A). We therefore investigated whether ORF52 possesses LLPS properties. We first analyzed the sphericity of ORF52 puncta in cells expressing mCherry-ORF52 or RFP-ORF52. ORF52 puncta were spherical, with sizes similar to those of cVACs (Fig. 2, A–C). ORF52 puncta exhibited liquid-like properties, as demonstrated by rapid fusion of two puncta upon encounter (Fig. 2 D). Furthermore, the fluorescence signal of ORF52 puncta recovered 50% within 1 min after photobleaching, indicating dynamic exchange of ORF52 proteins in cells (Fig. 2 E and Video 3).

To determine the function of ORF52 in cVACs formation, we took a genetic approach and transfected 293T cells with an MHV-68 ORF52-null BAC. We previously showed that viral gene expression (except *ORF52*) from this mutant BAC was normal, but virion assembly was arrested at the cytoplasmic maturation stage (Bortz et al., 2007). In the absence of ORF52, ORF33 and ORF45 were distributed diffusely in the cytoplasm (Fig. 2 F), in contrast to their punctate cytoplasmic distribution in cells infected with wild-type virus (Fig. 1, C and D). This indicates failure of cVACs formation. TEM ultrastructural analysis of cells transfected with the ORF52-null BAC confirmed the absence of cVACs, although immature viral particles were dispersed throughout the cell (Fig. 2 G). Together with our previous studies showing that tegumentation of ORF52-null particles is inefficient and incomplete (Bortz et al., 2007), these results strongly indicate that ORF52 is required for cVAC formation as well as complete tegumentation and secondary envelopment of viral particles.

Nucleic acids drive phase separation of ORF52

We previously solved the crystal structure of ORF52 (residues 1–102), which showed that the N terminus is structured and harbors dimerization and possibly tetramerization domains (Benach et al., 2007). ORF52 also contains an intrinsically disordered C terminus (Benach et al., 2007). Such a structure might efficiently mediate the phase separation of ORF52 without requiring any other components including proteins or nucleic acids. To test this, we purified from *Escherichia coli* ORF52 protein (Fig. S2 B), whose ratio of absorbance at 260–280 is 0.56, indicating that the purified ORF52 is free of contaminating nucleic acids. We then examined its ability to phase separate in vitro. No phase separation was observed in solution at the salt concentrations we tested, even when the ORF52 concentration was as high as 1 mM (Fig. S2 C). During viral infection, expression of ORF52 was detected at 12 hpi and later time points (Fig. S2 D), consistent with the formation of ORF52 puncta from 12 hpi on (Fig. 1 A). Quantitation results showed that the intracellular concentration of ORF52 at 12 hpi is ∼1 μM (Fig. S2 D). Taken together, these data indicate that additional cytosolic components are required to promote the phase separation of ORF52.

It was previously reported that Kaposi's sarcoma-associated herpesvirus (KSHV) ORF52 has DNA-binding ability which is essential for its inhibition of cGAS activity (Wu et al., 2015). We therefore examined whether double-stranded DNA oligonucleotides could induce phase separation of MHV-68 ORF52 in vitro. Upon mixing, ORF52 and DNA formed micrometer-sized liquid droplets, which were visible within 10 s (Fig. 3 A). Small droplets continuously fused into larger ones (Fig. 3 C and Video 4). Furthermore, recovery of fluorescent signals after photobleaching demonstrated the mobility of droplets (Fig. 3 D). Phase separation of ORF52 and DNA occurred when the concentration of each exceeded 1 μM, and aggregates were observed under many conditions (Fig. 3 E).

Analysis of γ-herpesvirus virion composition revealed that apart from the viral DNA genome, viral proteins, and lipids, RNA is also present in purified viral particles (Bechtel et al., 2005; Cliffe et al., 2009). We hypothesized that RNA might induce phase separation of ORF52 as well as DNA. To this end, phase separation assays were performed in vitro by mixing fluorescently labeled ORF52 protein with total cellular RNA in a buffer mimicking physiological ion concentrations. Similar to the result obtained from incubating ORF52 protein with DNA, ORF52 and RNA formed micrometer-sized liquid droplets within 10 s (Fig. 3 B). These droplets underwent fusion, and the fluorescent signal recovered after photobleaching (Fig. 3, F and G; and Video 5). Furthermore, RNA at low concentrations induced the formation of liquid droplets (Fig. 3 H). Total RNA extracted from either infected or uninfected cells induced phase separation of ORF52 (Fig. S2 F), indicating that viral RNA (v-mRNA, v-tRNA, or v-microRNA) may not be required for ORF52 phase separation. Nonetheless, we found that v-tRNAs could promote ORF52 phase separation in vitro (Fig. S2 E). Collectively, these results reveal that, in the absence of other viral proteins, phase separation of ORF52 is driven by nucleic acids in vitro.

Next, we tested which types of nucleic acid are recruited to cVACs during viral assembly in vivo. After infection by recombinant virus, cells were fixed and stained with DAPI. We found little DNA in the cytoplasm and no obvious accumulation of DNA in cVACs (Fig. 3 I). However, when cells were incubated with EU to label nascent RNA and then infected with

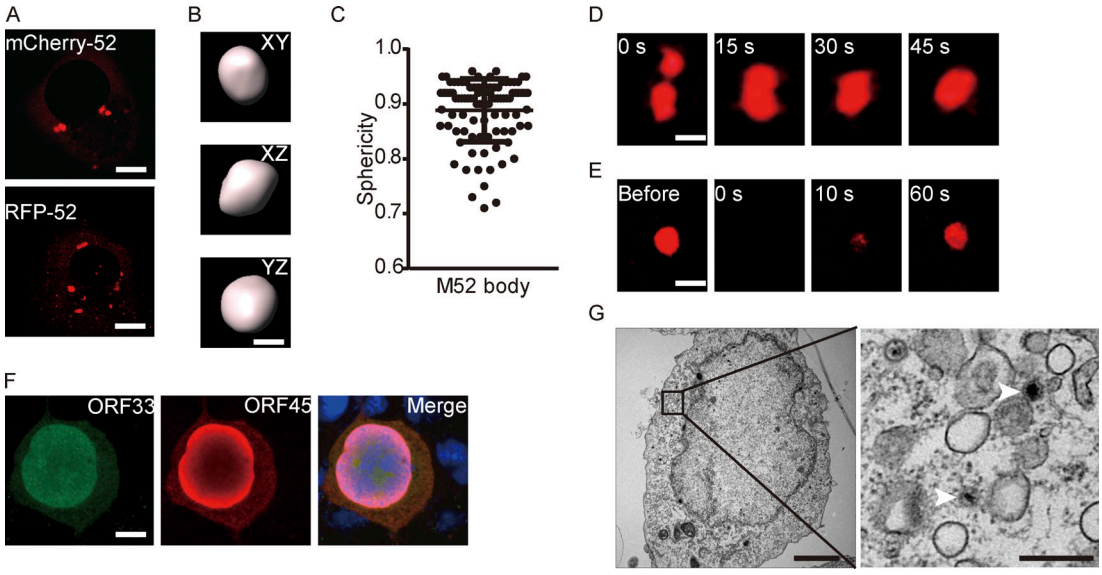

Figure 2. **ORF52 possesses LLPS properties and is required for cVACs formation. (A)** ORF52 forms puncta in COS-7 cells after transfection. Plasmids expressing RFP-ORF52 or mCherry-ORF52 were individually transfected into COS-7 cells. Cells were observed with a fluorescence microscope. Bar: 5 µm. **(B)** mCherry-labeled ORF52 forms spherical bodies in cells. The XY, XZ, and YZ planes of a representative ORF52 body are shown. Bar: 2 µm. **(C)** A plot showing the sphericity of ORF52 bodies (n = 94). Error bars represent SD. **(D)** Fusion of ORF52 puncta. Plasmids expressing mCherry-ORF52 were transfected into COS-7 cells. Cells were observed with a time-lapse microscope at 24 h post transfection. Bar: 2 µm. **(E)** FRAP of mCherry-ORF52 in COS-7 cells at 37°C. Bar: 2 µm. **(F)** Formation of cVACs relies on ORF52. 293T cells were transfected with ORF52-null BAC and detected by indirect immunofluorescence at 48 h post transfection. ORF33 was detected using a mouse anti-ORF33 monoclonal antibody, followed by an Alexa Fluor 488-conjugated secondary antibody (green channel). ORF45 was detected using a rabbit anti-ORF45 polyclonal antibody, followed by an Alexa Fluor 647-conjugated secondary antibody (red channel). Nuclei were stained with DAPI (blue channel). Bar: 5 µm. **(G)** TEM of a 293T cell transfected with ORF52-null BAC. The right panel shows an enlargement of the boxed area from the left panel. Scale bars: 3 µm (main image); 0.5 µm (zoomed-in image). White arrowheads: capsids.

recombinant virus, cytoplasmic nascent RNA was co-aggregated with ORF52 (Fig. 3 J), indicating that RNA is likely to promote LLPS of ORF52 during the late stage of viral replication.

The LLPS properties of ORF52 are critical for cVACs formation and virion production

We hypothesized that multivalent interactions between the oligomerization domains and between nucleic acids and the IDR are the driving forces underlying LLPS of ORF52. To test this idea, we constructed four ORF52 mutants (M1, M2, M3, and M4) with deletions of the α1-helix, α2-helix, α3-helix plus β sheet, or the IDR (Fig. 4 A and Fig. S3 A). None of the cells transfected with M1, M2, or M3 showed puncta in the cytoplasm, and only a few puncta formed in M4-transfected cells (Fig. 4, B and C). This suggests that the oligomerization domains and the IDR are all important for ORF52 phase separation. To investigate the functional significance of the LLPS properties of ORF52 during viral replication, we individually introduced these deletions into the viral genome and examined the replication efficiencies of viral mutants by analyzing viral genome copy numbers and viral titers in the cell culture supernatant. Our results showed that M1, M2, and M3 deletions all blocked production of mature virions (Fig. 4, D and E), consistent with our previous structural and functional studies demonstrating that the α1-α3 helices and the β sheet of ORF52 are all essential for its function and viral replication (Benach et al., 2007; Wang et al., 2012). Furthermore, the viral titer of the M4 mutant decreased more than two logs compared to that of WT, indicating that the C-terminal IDR of ORF52 also plays a critical role in viral replication (Fig. 4, D and E).

ORF52 is conserved among γ-herpesviruses. Sequence alignment of ORF52 homologues revealed that there is a highly conserved cluster of basic amino acids in the ORF52 IDR (Benach et al., 2007). Since many IDRs are enriched with positively charged amino acids, such as lysine (K) and arginine (R; Shin and Brangwynne, 2017), we tested whether this cluster is required for ORF52 phase separation. We introduced point mutations into the ORF52 expression plasmid and obtained mutants M5 (K120A/K121A), M6 (R122A/R123A), and M7 (K120A/K121A/R122A/R123A or 4A; Fig. 4 A and Fig. S3 A). After expressing these mutant proteins in cells, we compared their abilities to form puncta. The percentage of cells containing ORF52 puncta decreased significantly in cells expressing M5 or M7, although no obvious difference was observed in cells expressing M6 (Fig. 4, B and C). These results indicated that this cluster, in particular K120/K121, plays a critical role in mediating the phase separation of ORF52. Accordingly, viral mutants harboring M5 or M7 displayed significant deficiencies in viral replication and virus production, as shown by viral genome copy numbers and viral titers (Fig. 4, D and E).

We further investigated the abilities of these mutants to form cVACs. In cells transfected with WT or M6 BAC, clusters of naked capsids were seen within the cytoplasm, and tegumentation and envelopment of capsids took place successfully, yielding mature virions enclosed within vesicles (Fig. 4 F). Confocal imaging data showed that tegument proteins ORF33

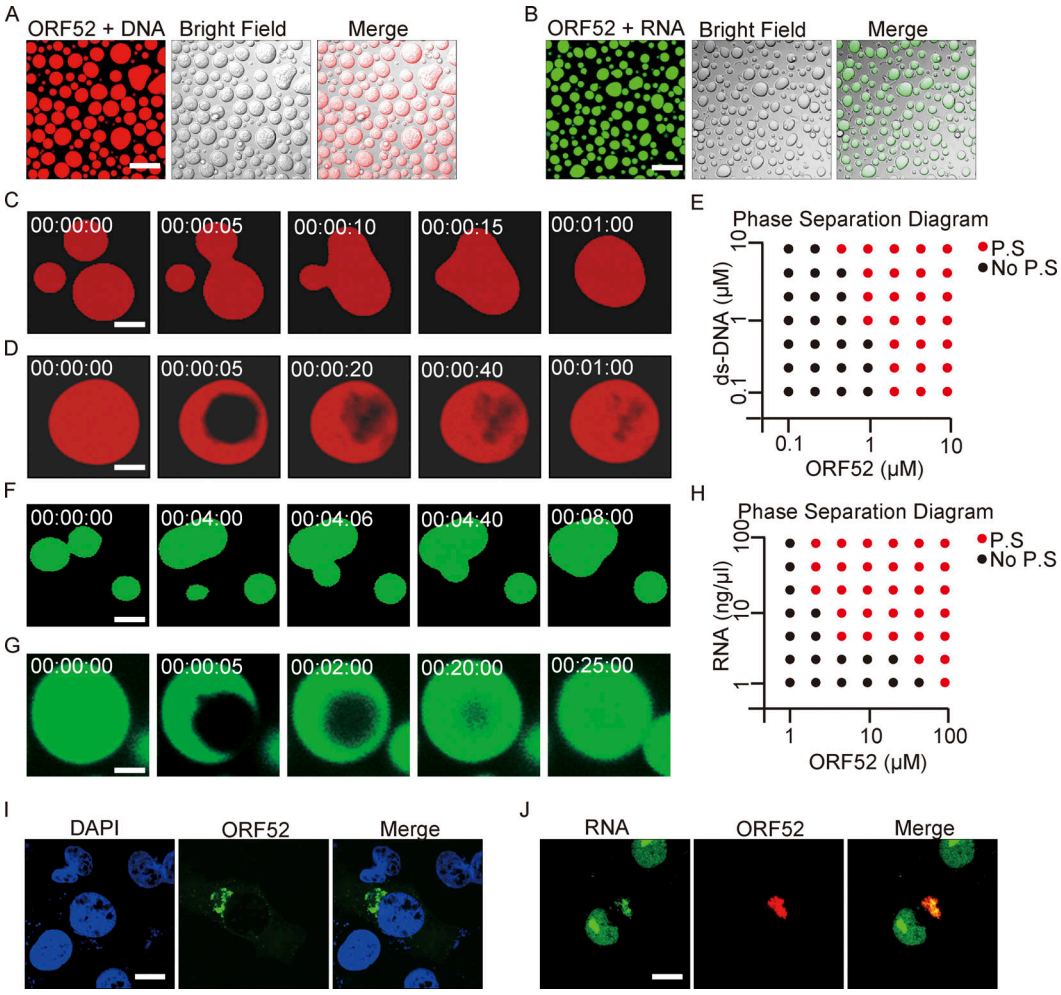

Figure 3. **Nucleic acids drive phase separation of ORF52. (A)** In vitro phase separation assay of ORF52 with DNA. Phase separation of ORF52 with 45-bp ds-DNA was performed in 20 mM Tris-HCl, pH 7.5, 150 mM NaCl. 10 μM ORF52 protein was mixed with 5 μM 45-bp ds-DNA (2% Cy3-labeled) in 96-well plates coated with 20 mg/ml BSA. Mixtures were incubated and images were captured by confocal microscopy. Bar: 20 μm. **(B)** ORF52 phase separation in vitro in the presence of total RNA isolated from COS-7 cells. Phase separation of ORF52 with total RNA was performed in physiological buffer. 5 μM ORF52 protein (3% Alexa 488-labeled) was mixed with 100 ng/μl total RNA in 96-well plates coated with 20 mg/ml BSA. Mixtures were incubated and images were captured by confocal microscopy. Bar: 10 μm. **(C)** Fusion of ORF52-DNA droplets formed during the in vitro phase separation process. Bar: 5 μm. **(D)** FRAP of ORF52-DNA liquid droplets. Bleaching was performed during the in vitro phase separation process. **(E)** Phase separation diagram of ORF52 with ds-DNA. Bar: 5 μm. **(F)** Fusion of ORF52-RNA droplets formed during the in vitro phase separation process. Bar: 5 μm. **(G)** FRAP of ORF52-RNA liquid droplets. Bleaching was performed during the in vitro phase separation process. Bar: 5 μm. **(H)** Phase separation diagram of ORF52 with total cellular RNAs. **(I)** cVACs contain little DNA. After infection with mEosEM-ORF52 virus (MOI = 3), COS-7 cells were fixed and stained with DAPI. Bar: 5 μm. **(J)** RNA is concentrated in cVACs. EU was added to cultured COS-7 cells to label nascent RNA 24 h before the cells were infected with mCherry-ORF52 virus. EU-labeled RNA was detected by click chemistry reaction. Bar: 5 μm.

and ORF45 were also co-aggregated with the puncta in the cytoplasm in cells transfected with M6 BAC (Fig. S3 B). These observations indicated formation of cVACs. However, only capsids but no mature virions were seen in cells transfected with M1, M2, or M3 BAC, and no co-aggregation of ORF33 and ORF45 in the cytoplasm was observed, consistent with the complete loss of ORF52 phase separation properties in these mutants (Fig. 4 F and Fig. S3 B). cVACs structures were still detected in cells with M4, M5, or M7 mutant virus, although the frequency of cVACs occurrence decreased markedly (Fig. 4 F and Fig. S3 B). These results indicate that LLPS of ORF52 is critical for cVACs formation and consequently production of mature virions.

Because ORF52 is a conserved tegument protein among γ-herpesviruses, we also examined whether its homologues in KSHV and Epstein-Barr virus (EBV) have phase separation properties. Similar to MHV68-ORF52, KSHV-ORF52, and EBV-BLRF2 formed puncta in transfected COS-7 cells, and their liquid-like behavior was confirmed by FRAP (Fig. S3, C and D). Moreover, we confirmed that the conserved cluster of basic amino acids in the ORF52 IDR is also important for phase separation of KSHV-ORF52 and EBV-BLRF2 in cells (Fig. S3 E). Our previous work showed that KSHV-ORF52 and EBV-BLRF2 can substitute for the function of MHV68-ORF52 in viral replication (Wang et al., 2012). Thus, we hypothesized that ORF52

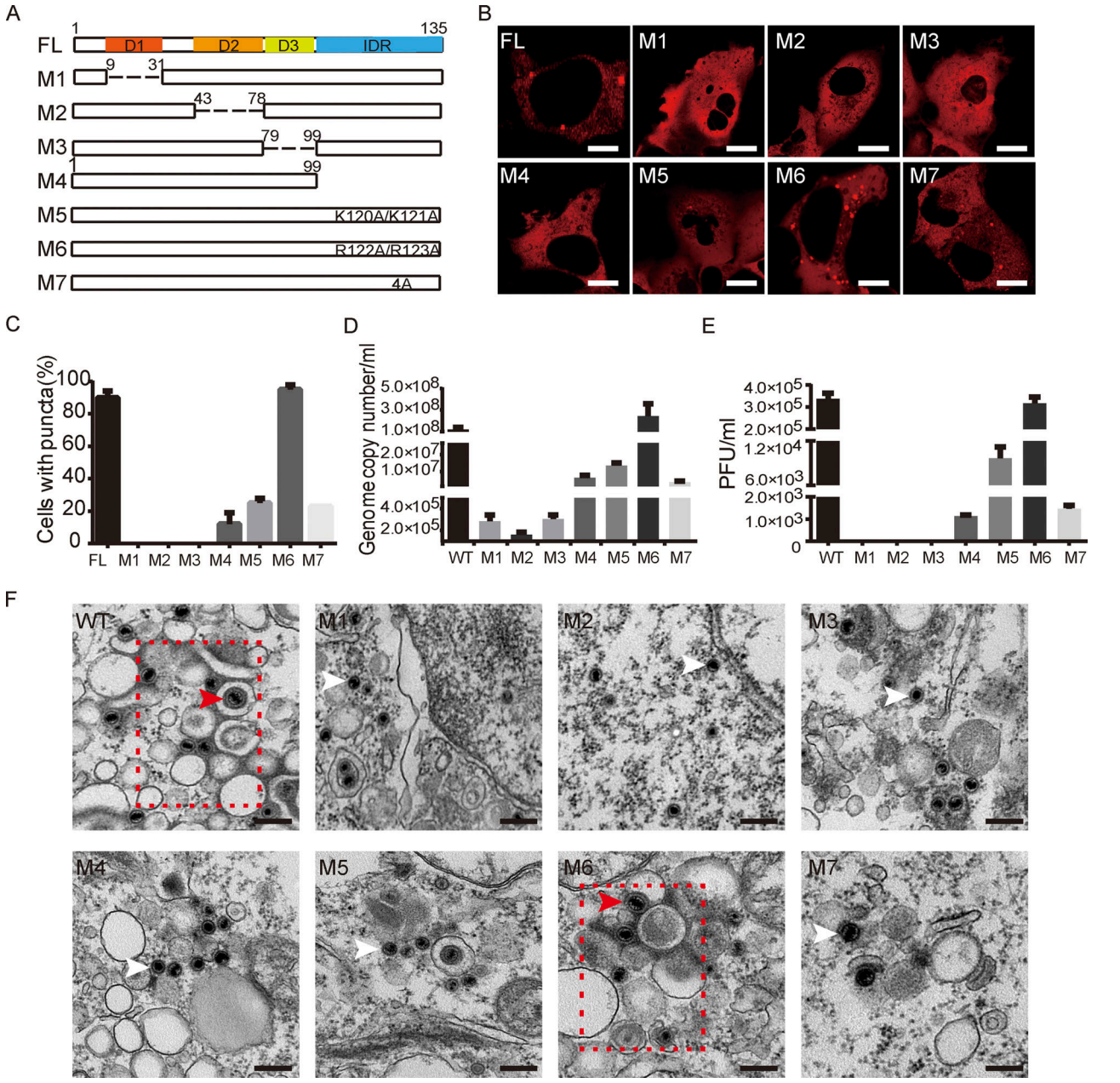

Figure 4. **The LLPS properties of ORF52 are critical for cVACs formation and virion production. (A)** Schematic presentation of full-length and mutant ORF52 proteins. **(B and C)** ORF52 mutants have different phase separation properties. Plasmids expressing mCherry-ORF52 or mCherry-tagged mutants were individually transfected into COS-7 cells. Cells were observed with a fluorescent microscope at 24 h post transfection (B). Bar: 5 µm. In each experiment, 30 cells expressing mCherry-ORF52 or mutants were randomly chosen. Cells with ORF52 puncta were counted, and the percentage of cells with ORF52 puncta among all cells expressing fluorescent protein was calculated (C). Values shown are means ± SD (n = 3). **(D and E)** Phase separation of ORF52 is critical for complete viral replication and mature virion formation. WT BAC or BAC containing the indicated ORF52 mutation was transfected individually into 293T cells. After 96 h, viral genome copies in the supernatant were determined by real-time PCR (D) and viral titers were examined by plaque formation assay (E). Values shown are means ± SD (n = 3). **(F)** ORF52 phase separation is required for cVACs formation. 293T cells were individually transfected with WT BAC or BAC harboring the indicated ORF52 mutation. cVAC structure was analyzed by TEM. Bar: 0.2 µm. Red boxes: cVACs; white arrowheads: capsids or immature viral particles; red arrowheads: mature viral particles.

homologues possess the ability to drive cVACs formation by phase separation in complementation assays. In agreement with this, we found that KSHV-ORF52 forms cVACs together with other tegument proteins, such as ORF33, while cVAC was not observed when the phase separation behavior of KSHV-ORF52 was impaired (Fig. S3, F and G).

Tegument proteins are multifunctional during the herpesvirus life cycle. As structural components of virions, they are released into the cytoplasm of infected cells upon virus entry and play important regulatory roles during early infection. Indeed, we and others have recently also shown that ORF52 effectively targets cGAS-DNA condensation through DNA-induced

LLPS during the early stage of viral infection (Bhowmik et al., 2021; Xu et al., 2021). However, it is worth noting that 293T cells are deficient in the cGAS-STING pathway (Sun et al., 2013). Therefore, the phenotypes we observed in this study (Fig. 4, D–F) can be mostly attributed to deficiencies in the formation of ORF52-RNA biomolecular condensates and cVACs, and hence impaired virion assembly, during the late stage of viral replication.

In summary, our work defines herpesvirus cVACs as membraneless compartments that are generated through LLPS. This process is mediated by an abundant tegument protein. Our result adds to the cellular processes that are facilitated by phase separation. It also provides novel insights into cVACs biogenesis and lays a foundation for further investigation of the complete details of herpesvirion morphogenesis.

Materials and methods

Cell culture and transfection

HEK293T cells, BHK-21 cells and COS-7 cells were cultured in DMEM (Gibco) supplemented with 10% (v/v) FBS (HyClone), 50 units/ml penicillin and 50 µg/ml streptomycin. All cells were cultured at 37°C in a humidified atmosphere containing 5% CO_2. Expression plasmids were transfected into COS-7 cells with Lipofectamine 3000 (Invitrogen) or transfected into 293T cells with jetPEI (Polyplus).

Antibodies and small molecules

Mouse mAbs against ORF33 (1:200 dilution for immunofluorescence assay), rabbit mAbs against ORF52 (1:2,000 dilution for Western blotting), rabbit polyclonal antibody against ORF38 (1:200 dilution for immunofluorescence), and rabbit polyclonal antibody against ORF45 (1:200 dilution for immunofluorescence) were produced in our lab. Mouse mAbs against mCherry (#TA-07; 1:2,000 dilution for Western blotting) was from ZSGB-BIO. Mouse mAbs against actin (#ab3280; 1:2,000 dilution for Western blotting) was from Abcam. Propylene glycol (#A501754) was from Sangon Biotech. Goat secondary antibodies against mouse IgG conjugated with Alexa Fluor 488 (#A11029) and goat secondary antibodies against rabbit IgG conjugated with Alexa Fluor 647 (#A21244) were from Invitrogen. All secondary antibodies were diluted at 1:1,000 for immunofluorescence assays.

Viruses

MHV-68 viruses were propagated by infecting BHK-21 cells. About 4 d post infection (pi), the supernatant was harvested and cleared of large cellular debris by centrifugation. To measured viral titers, monolayers of BHK-21 cells were infected with virus for 1 h and overlaid with 1% methylcellulose (Sigma) for 5 d. Cells were fixed and stained with 0.2% crystal violet (in 20% ethanol), and plaques were then counted to determine the titer.

Construction of plasmids for mammalian expression

mCherry-ORF52 plasmid was constructed by inserting mCherry cDNA and ORF52 (MHV68, KSHV, or EBV) cDNA into pCI-3flag vector. RFP-ORF52(MHV68) plasmid was constructed in pCMV-HA vector. KSHV-ORF52 and EBV-BLRF2 plasmids were constructed in pCI-3flag vector. All mutants were constructed using a site-directed mutagenesis kit. pTAG-ORF33, pTAG-ORF38, pTAG-ORF42, pTAG-ORF45, pTAG-ORF52, pTAG-ORF55, pTAG-ORF64a, pTAG-ORF64b, pTAG-ORF75a, pTAG-ORF75b, and pTAG-ORF75c were kindly provided by Dr. Ren Sun (University of California, Los Angeles, Los Angeles, CA).

Generation of recombinant MHV-68

All recombinant constructs, including BAC-mCherry-ORF52, BAC-mEosEM-ORF52, BAC-ORF52-M1, BAC-ORF52-M2, BAC-ORF52-M3, BAC-ORF52-M4, BAC-ORF52-M5, BAC-ORF52-M6, and BAC-ORF52-M7, were generated as described previously (Wu et al., 2011). Briefly, the Kan/I-SceI cassettes were amplified from template by PCR with primers. The purified PCR fragment was electroporated into competent *E. coli* SHG68 cells. The recombinant clones were selected at 32°C on LB plates containing 34 µg/ml chloramphenicol and 50 µg/ml kanamycin and then characterized by PCR. Positive clones were induced at 42°C and plated on LB plates containing 1% *L*-arabinose for secondary recombination. Clones were picked from *L*-arabinose plates onto plates with kanamycin and onto plates with chloramphenicol. The kanamycin-sensitive clones were second-recombinant clones and confirmed by RFLP (restriction fragment length polymorphism) analysis and sequencing.

To propagate the recombinant MHV-68 viruses, the desired recombinant BACs were transfected into 293T cells, and supernatant from each transfection was collected to infect new BHK-21 cells. Virus titer was determined by plaque assay.

E. coli strains, protein expression, purification, and labeling

E. coli BL21 (DE3) cells were used in this study for production of recombinant proteins. Cells were cultured in lysogeny broth (LB) medium at 37°C, 220 rpm. The coding sequence of MHV-68 ORF52 was inserted into a modified pRSFDuet-1 plasmid, harboring an N-terminal His6-SUMO tag, followed by an ubiquitin-like protease (ULP1) cleavage site. ORF52 protein was expressed and purified in the BL21(DE3) cell strain. Cell cultures were grown at 37°C until they reached optimal density (OD600 = 0.8). The temperature was then shifted to 16°C and the cells were induced with 0.5 mM β-D-1-thiogalactopyranoside (IPTG) overnight.

The cells were collected and lysed with a high-pressure cracker in lysis buffer (50 mM Tris-HCl, pH 7.5, 500 mM NaCl, 20 mM imidazole, 0.035% β-ME, 5% glycerol). After centrifugation, the supernatant was loaded onto a Ni-NTA affinity column and the proteins were eluted with elution buffer (50 mM Tris-HCl, pH 7.5, 500 mM NaCl, 500 mM imidazole, 0.035% β-ME, 5% glycerol). The His6-SUMO tag was cleaved by ULP1 at 4°C for about 4 h. The cleaved protein samples were further applied to a 5-ml Hitrap Heparin column (GE Healthcare) with a linear NaCl gradient from 300 mM to 1 M to remove the His6-SUMO tag and nucleic acids. Eluted protein was subjected to gel filtration on a 16/60 G200 Superdex column in 20 mM Tris-HCl, pH 7.5, 300 mM NaCl and 1 mM DTT. The peak sample was concentrated, measured, and stored at −80°C before use. Purified ORF52 protein was labeled with Alexa Fluor 488 by using an Alexa Fluor 488 Protein Labeling Kit (Thermo Fisher Scientific).

In vitro LLPS assay

Phase separation of ORF52 with 45-bp dsDNA (2% Cy3-labeled) was performed in 150 mM NaCl, 20 mM Tris-HCl, pH 7.5, with the indicated protein and DNA concentrations. Phase separation of ORF52 (3% Alexa Fluor 488-labeled) with total RNA was performed in physiological buffer (20 mM Tris-HCl, pH 7.5, 15 mM NaCl, 135 mM KCl, 1.5 mM $MgCl_2$). For FRAP and time-lapse imaging experiments, phase separation assays were carried out in 96-well plates (Corning) coated with 20 mg/ml BSA (Sigma-Aldrich) then washed with Milli-Q H_2O three times.

Live-cell imaging

Cells were grown on glass-bottom cell-culture dishes (801002; Nest), and images were taken with an Olympus FV1200 confocal microscopy system using a 100× oil objective (NA = 1.49). Cells were imaged on a heated stage (37°C) and supplemented with warmed humidified air containing 5% CO_2. Fluorescence images were captured at indicated time points using FV10-ASW3.1 software.

Immunofluorescence cell staining

Cells were seeded on glass coverslips in a 24-well plate and grown overnight. Cells were infected with MHV-68 and fixed at 24 hpi. After 4% PFA fixation for 15 min at room temperature, cells were permeabilized with 0.2% Triton X-100 and blocked with 5% normal goat serum. Diluted mouse anti-ORF33 antibody and rabbit anti-ORF45 and anti-ORF38 antibodies were applied to the coverslips and incubated overnight at 4°C. After PBS washing, corresponding fluorescently labeled secondary antibodies were applied at room temperature for 1 h and further washed with PBS. After mounting with DAPI, the slides were examined under the fluorescence microscope (Olympus).

CLEM

CLEM imaging was performed by following the protocol as previously reported (Fu et al., 2020). Briefly, cultured cells infected with recombinant MHV-68 virus mEosEM-ORF52 were collected at 24 hpi and centrifuged to obtain cell pellets. The pelleted cells were fixed using 4% paraformaldehyde and 2.5% glutaraldehyde in 100 mM PBS, pH 7.2, at 4°C for 12 h. After postfixation with 1% OsO_4 and staining with 2% uranyl acetate, cells were dehydrated with increasing concentrations of ethanol. Cells were infiltrated and embedded in 100% Epon resin and cut into 100-nm ultrathin Epon sections. Fluorescence images and DIC images were acquired using a confocal microscopy system. The same section identified from the DIC images was imaged by a FEI Tecnai Spirit TEM operated at 120 kV. Detailed subcellular EM images were acquired with a MORADA G3 camera. Registration of fluorescence images and EM images was performed by eC-CLEM using gold nanoparticles as fiducial makers.

FRAP

FRAP assays were performed using the FRAP module of the Olympus FV1200 confocal microscopy system with a 100× oil objective. ORF52 bodies (in vivo) or ORF52 droplets (in vitro) were bleached using a 473-nm laser beam. Bleaching was focused on a circular region of interest (ROI) using 100% laser power. Time-lapse images were collected. The fluorescence intensity of the photobleached area was normalized to the intensity of the unbleached area. GraphPad Prism was used to plot and analyze the FRAP results.

3D rendering and sphericity measurement

COS-7 cells transiently transfected with mCherry-ORF52 or infected with viruses were fixed with 4% PFA. Sequential images were acquired using a confocal microscope (Olympus FV1200) with a 100× oil objective. The step size along the Z axis was 0.2 µm. Confocal image stacks were rendered into 3D volumes and analyzed using Imaris v9 (Bitplane AG) with the surface tool.

Transmission electron microscopy

Virus assembly and particle morphology were examined by TEM as previously described (Bortz et al., 2007). 293T cells were individually transfected with WT, ORF52-null or other mutant BACs as indicated. At 4-d post transfection, the cells were fixed in 2.5% glutaraldehyde (Sigma) in PBS at 4°C for 24 h, postfixed in 1% OsO_4, dehydrated, and embedded in Epon. Approximately 70-nm ultrathin sections were stained with 2% uranyl acetate and 0.3% lead citrate and examined by a FEI Tecnai Spirit TEM operated at 120 kV.

Western blotting and estimation of ORF52 concentrations in infected cells

For Western blotting, cells were collected and lysed in cell lysis buffer (1% Triton X-100 [Sigma-Aldrich], 150 mM NaCl, 50 mM Tris-HCl [Amresco], pH 7.4), and equal amounts of protein were loaded onto an SDS-PAGE gel. Western blots were imaged by SageCapture (SAGECREATION) and quantified using Image J software.

Based on Western blot result, we quantified the amount of ORF52 protein in infected cells (equivalent to extract from 10^5 cells). The volume of each cell is ~4×10^{-12} L. Thus, the cytoplasmic concentration equals mass (ng) × 10^{-9}/(10^5 × 15,000 × 4×10^{-12}) M. The concentration of ORF52 at each time points post infection was estimated to be 0 µM (0 hpi), 0 µM (6 hpi), 1 µM (12 hpi), 6 µM (24 hpi), and 14 µM (36 hpi).

Online supplemental material

Fig. S1 shows the construction and analyses of recombinant MHV-68 viruses, related to Fig. 1. Fig. S2 shows phase separation properties of ORF52, related to Figs. 2 and 3. Fig. S3 shows the analyses of ORF52 mutants and the LLPS properties of ORF52 from other γ-herpesviruses, related to Fig. 4. Table S1 shows all nucleic acid sequences used in this work. Video 1 shows cVAC formation in a cell, related to Fig. 1. Video 2 shows FRAP of a cVAC in a cell, related to Fig. 1. Video 3 shows FRAP of ORF52 puncta in cells, related to Fig. 2. Video 4 shows ORF52-DNA phase separation in vitro, related to Fig. 3. Video 5 shows ORF52-RNA phase separation in vitro, related to Fig. 3.

Acknowledgments

We thank Dr. Dong Li for providing COS-7 cells, Drs. Hong Zhang and Chuanhui Han and members of the Deng laboratory

for helpful discussions, and Dr. Isabel Hanson for editing work. We also thank Ms. Yan Teng, Ms. Shuoguo Li, and Ms. Yun Feng as well as Ms. Can Peng at the Center for Biological Imaging, Institute of Biophysics for help with confocal imaging and TEM, respectively.

This work was supported by grants from the National Natural Science Foundation of China (81630059, 81325012, and 81921005), the Ministry of Science and Technology (2016YFA0502101), and the Chinese Academy of Sciences (KJZD-SW-L05, XDB37030205, and XDB37040301).

The authors declare no competing financial interests.

Author contributions: S. Zhou and H. Deng designed experiments. S. Zhou, Z. Fu, Z. Zhang, G. Xu, and L. Sun performed experiments. X. Jia and F. Sun contributed reagents. S. Zhou, P. Gao, P. Xu and H. Deng analyzed data. S. Zhou and H. Deng wrote and revised the manuscript.

Submitted: 25 January 2022
Revised: 19 July 2022
Accepted: 30 September 2022

References

Banani, S.F., H.O. Lee, A.A. Hyman, and M.K. Rosen. 2017. Biomolecular condensates: Organizers of cellular biochemistry. *Nat. Rev. Mol. Cell Biol.* 18:285–298. https://doi.org/10.1038/nrm.2017.7

Bechtel, J., A. Grundhoff, and D. Ganem. 2005. RNAs in the virion of Kaposi's sarcoma-associated herpesvirus. *J. Virol.* 79:10138–10146. https://doi.org/10.1128/JVI.79.16.10138-10146.2005

Benach, J., L. Wang, Y. Chen, C.K. Ho, S. Lee, J. Seetharaman, R. Xiao, T.B. Acton, G.T. Montelione, H. Deng, et al. 2007. Structural and functional studies of the abundant tegument protein ORF52 from murine gammaherpesvirus 68. *J. Biol. Chem.* 282:31534–31541. https://doi.org/10.1074/jbc.M705637200

Bhowmik, D., M. Du, Y. Tian, S. Ma, J. Wu, Z. Chen, Q. Yin, and F. Zhu. 2021. Cooperative DNA binding mediated by KicGAS/ORF52 oligomerization allows inhibition of DNA-induced phase separation and activation of cGAS. *Nucleic Acids Res.* 49:9389–9403. https://doi.org/10.1093/nar/gkab689

Boeynaems, S., S. Alberti, N.L. Fawzi, T. Mittag, M. Polymenidou, F. Rousseau, J. Schymkowitz, J. Shorter, B. Wolozin, L. Van Den Bosch, et al. 2018. Protein phase separation: A new phase in cell biology. *Trends Cell Biol.* 28:420–435. https://doi.org/10.1016/j.tcb.2018.02.004

Bortz, E., L. Wang, Q. Jia, T.T. Wu, J.P. Whitelegge, H. Deng, Z.H. Zhou, and R. Sun. 2007. Murine gammaherpesvirus 68 ORF52 encodes a tegument protein required for virion morphogenesis in the cytoplasm. *J. Virol.* 81:10137–10150. https://doi.org/10.1128/JVI.01233-06

Bortz, E., J.P. Whitelegge, Q. Jia, Z.H. Zhou, J.P. Stewart, T.T. Wu, and R. Sun. 2003. Identification of proteins associated with murine gammaherpesvirus 68 virions. *J. Virol.* 77:13425–13432. https://doi.org/10.1128/jvi.77.24.13425-13432.2003

Cliffe, A.R., A.A. Nash, and B.M. Dutia. 2009. Selective uptake of small RNA molecules in the virion of murine gammaherpesvirus 68. *J. Virol.* 83:2321–2326. https://doi.org/10.1128/JVI.02303-08

Cortese, M., S. Goellner, E.G. Acosta, C.J. Neufeldt, O. Oleksiuk, M. Lampe, U. Haselmann, C. Funaya, N. Schieber, P. Ronchi, et al. 2017. Ultrastructural characterization of Zika virus replication factories. *Cell Rep.* 18:2113–2123. https://doi.org/10.1016/j.celrep.2017.02.014

Du Toit, A. 2020. Coronavirus replication factories. *Nat. Rev. Microbiol.* 18:411. https://doi.org/10.1038/s41579-020-0406-z

Fu, Z., D. Peng, M. Zhang, F. Xue, R. Zhang, W. He, T. Xu, and P. Xu. 2020. mEosEM withstands osmium staining and Epon embedding for super-resolution CLEM. *Nat. Methods.* 17:55–58. https://doi.org/10.1038/s41592-019-0613-6

Guo, H., S. Shen, L. Wang, and H. Deng. 2010. Role of tegument proteins in herpesvirus assembly and egress. *Protein Cell.* 1:987–998. https://doi.org/10.1007/s13238-010-0120-0

Guo, H., L. Wang, L. Peng, Z.H. Zhou, and H. Deng. 2009. Open reading frame 33 of a gammaherpesvirus encodes a tegument protein essential for virion morphogenesis and egress. *J. Virol.* 83:10582–10595. https://doi.org/10.1128/JVI.00497-09

Jia, X., S. Shen, Y. Lv, Z. Zhang, H. Guo, and H. Deng. 2016. Tegument protein ORF45 plays an essential role in virion morphogenesis of murine gammaherpesvirus 68. *J. Virol.* 90:7587–7592. https://doi.org/10.1128/JVI.03231-15

Lv, Y., S. Zhou, S. Gao, and H. Deng. 2019. Remodeling of host membranes during herpesvirus assembly and egress. *Protein Cell.* 10:315–326. https://doi.org/10.1007/s13238-018-0577-9

Mitrea, D.M., and R.W. Kriwacki. 2016. Phase separation in biology; functional organization of a higher order. *Cell Commun. Signal.* 14:1. https://doi.org/10.1186/s12964-015-0125-7

Owen, D.J., C.M. Crump, and S.C. Graham. 2015. Tegument assembly and secondary envelopment of alphaherpesviruses. *Viruses.* 7:5084–5114. https://doi.org/10.3390/v7092861

Paul, D., V. Madan, and R. Bartenschlager. 2014. Hepatitis C virus RNA replication and assembly: Living on the fat of the land. *Cell Host Microbe.* 16:569–579. https://doi.org/10.1016/j.chom.2014.10.008

Peng, L., S. Ryazantsev, R. Sun, and Z.H. Zhou. 2010. Three-dimensional visualization of gammaherpesvirus life cycle in host cells by electron tomography. *Structure.* 18:47–58. https://doi.org/10.1016/j.str.2009.10.017

Procter, D.J., A. Banerjee, M. Nukui, K. Kruse, V. Gaponenko, E.A. Murphy, Y. Komarova, and D. Walsh. 2018. The HCMV assembly compartment is a dynamic Golgi-derived MTOC that controls nuclear rotation and virus spread. *Dev. Cell.* 45:83–100.e7. https://doi.org/10.1016/j.devcel.2018.03.010

Shen, S., X. Jia, H. Guo, and H. Deng. 2015. Gammaherpesvirus tegument protein ORF33 is associated with intranuclear capsids at an early stage of the tegumentation process. *J. Virol.* 89:5288–5297. https://doi.org/10.1128/JVI.00079-15

Shin, Y., and C.P. Brangwynne. 2017. Liquid phase condensation in cell physiology and disease. *Science.* 357:eaaf4382. https://doi.org/10.1126/science.aaf4382

Sun, L., J. Wu, F. Du, X. Chen, and Z.J. Chen. 2013. Cyclic GMP-AMP synthase is a cytosolic DNA sensor that activates the type I interferon pathway. *Science.* 339:786–791. https://doi.org/10.1126/science.1232458

Vidick, S., B. Leroy, L. Palmeira, B. Machiels, J. Mast, S. Francois, R. Wattiez, A. Vanderplasschen, and L. Gillet. 2013. Proteomic characterization of murid herpesvirus 4 extracellular virions. *PloS One.* 8:e83842. https://doi.org/10.1371/journal.pone.0083842

Wang, L., H. Guo, N. Reyes, S. Lee, E. Bortz, F. Guo, R. Sun, L. Tong, and H. Deng. 2012. Distinct domains in ORF52 tegument protein mediate essential functions in murine gammaherpesvirus 68 virion tegumentation and secondary envelopment. *J. Virol.* 86:1348–1357. https://doi.org/10.1128/JVI.05497-11

White, S., H. Kawano, N.C. Harata, and R.J. Roller. 2020. Herpes simplex virus organizes cytoplasmic membranes to form a viral assembly center in neuronal cells. *J. Virol.* 94:e00900-20. https://doi.org/10.1128/JVI.00900-20

Wu, J.J., W. Li, Y. Shao, D. Avey, B. Fu, J. Gillen, T. Hand, S. Ma, X. Liu, W. Miley, et al. 2015. Inhibition of cGAS DNA sensing by a herpesvirus virion protein. *Cell Host Microbe.* 18:333–344. https://doi.org/10.1016/j.chom.2015.07.015

Wu, T.T., H.I. Liao, L. Tong, R.S. Leang, G. Smith, and R. Sun. 2011. Construction and characterization of an infectious murine gammaherpesivrus-68 bacterial artificial chromosome. *J. Biomed. Biotechnol.* 2011:926258. https://doi.org/10.1155/2011/926258

Xu, G., C. Liu, S. Zhou, Q. Li, Y. Feng, P. Sun, H. Feng, Y. Gao, J. Zhu, X. Luo, et al. 2021. Viral tegument proteins restrict cGAS-DNA phase separation to mediate immune evasion. *Mol. Cell.* 81:2823–2837.e9. https://doi.org/10.1016/j.molcel.2021.05.002

Zhao, Y.G., and H. Zhang. 2020. Phase separation in membrane biology: The interplay between membrane-bound organelles and membraneless condensates. *Dev. Cell.* 55:30–44. https://doi.org/10.1016/j.devcel.2020.06.033

JCB

Supplemental material

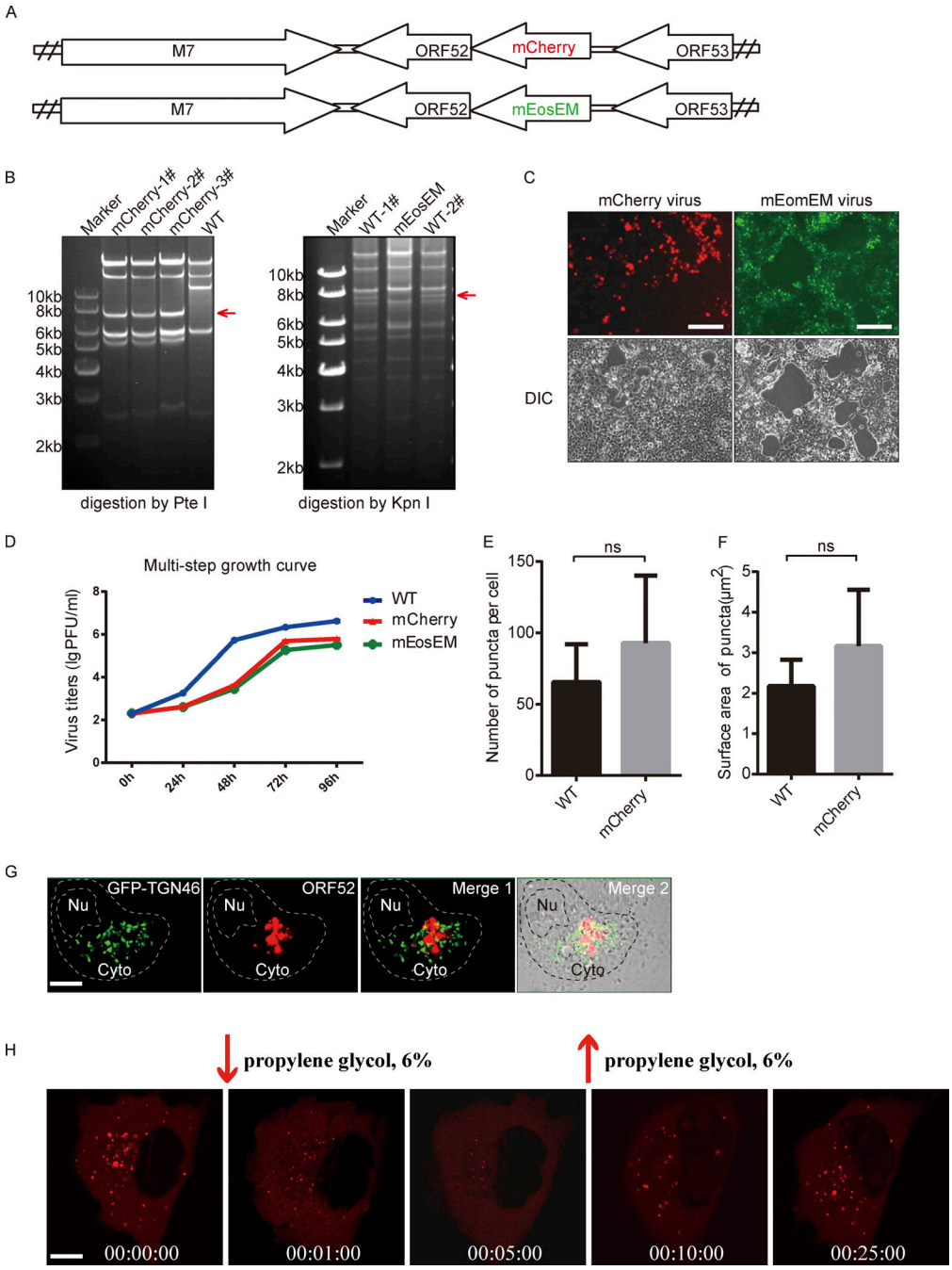

Figure S1. **Construction and analyses of recombinant MHV-68 viruses. (A)** A schematic diagram of mCherry-ORF52 BAC and mEosEM-ORF52 BAC constructs. **(B)** Left panel: WT BAC DNA and mCherry-ORF52 BAC DNA were isolated from *E. coli* strain SHG68 (GS1783). The DNAs were digested with PteI. The arrow indicates the position of a 7.8-kb PteI fragment resulting from *mCherry* insertion. Right panel: WT BAC DNA and mEosEM-ORF52 BAC DNA were isolated from *E. coli* strain SHG68 (GS1783). The DNAs were digested with KpnI. The arrow indicates the position of a 7.7-kb KpnI fragment which disappeared as a result of *mEosEM* insertion. **(C)** 293T cells were individually transfected with mCherry-ORF52 BAC or mEosEM-ORF52 BAC and images were captured by a fluorescence microscope. Bright-field images of the same area are shown on the bottom. Bar: 200 μm. **(D)** Multi-step growth curves of the recombinant viruses. BHK cells were infected with the indicated viruses at an MOI = 0.05 and cultured for 4 d. Viral titers were examined at the indicated time points. Values shown are means ± SD (n = 3). **(E and F)** Quantification of cytoplasmic ORF52 puncta in COS-7 cells infected by WT virus or mCherry-ORF52 virus. COS-7 cells were infected with WT virus or mCherry-ORF52 virus at a MOI of 3 and fixed at 18 hpi. Number of ORF52 puncta per cell (E) and mean surface areas of puncta (F) were measured using the microscopy image analysis software, Imaris. Error bar represents SD. Statistical analyses were performed using a two-tailed non-parametric t test. Data were collected from at least three independent experiments. **(E)** WT, n = 6; mCherry, n = 7. **(F)** WT, n = 6; mCherry, n = 5. **(G)** Analysis of co-localization of ORF52 with TGN. A plasmid expressing GFP-TGN46 was transfected into COS-7 cells. At 12 h post transfection, COS-7 cells were infected with mCherry-ORF52 virus. Cells were fixed at 24 hpi and observed with a confocal microscope (FV1200). Shown are the merged images of GFP-TGN signals (green) and mCherry-ORF52 signals (red) without the bright-field image (Merge 1) or with the bright-field image (Merge 2). Nu, nucleus. Bar: 5 μm. **(H)** Fluorescent images of COS-7 cells infected with mCherry-ORF52 virus at an MOI = 3 and treated with 6% propylene glycol (PG) at 24 hpi. Bar: 5 μm. Source data are available for this figure: SourceData FS1.

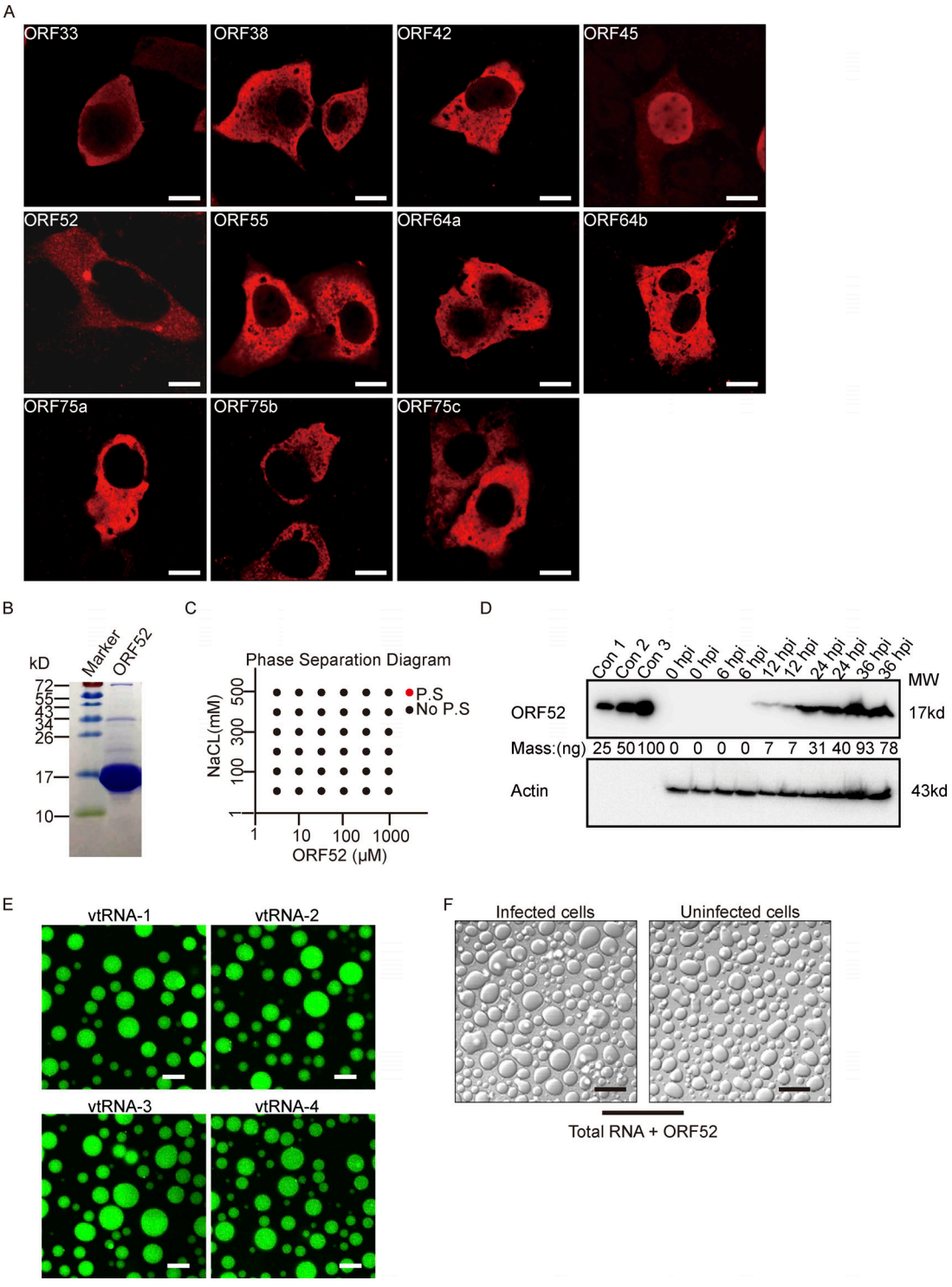

Figure S2. **Analyses of ORF52 phase separation. (A)** Plasmids expressing different tegument proteins were individually transfected into COS-7 cells. At 24 h post transfection, the cells were fixed with 4% paraformaldehyde and then permeabilized with 0.2% Triton X-100. Indirect immunofluorescence analysis was carried out using an antibody against HA-tag or Flag-tag. Bar: 5 μm. **(B)** Purity of bacterially expressed ORF52, analyzed by Coomassie blue staining. **(C)** Phase separation diagram of ORF52 at the indicated concentrations. ORF52 with the indicated concentrations were incubated in phase separation assay buffer with different concentrations of NaCl and visualized by confocal microscopy. P.S, phase separation. **(D)** Expression levels of ORF52 in 293T cells after MHV-68 infection (MOI = 3) at different hours post infection, as examined by Western blotting. con1-3: Bacterially expressed and purified ORF52 proteins were loaded at the indicated amount to draw standard curve. **(E)** Phase separation assay of ORF52 with v-tRNA was performed in physiological buffer. 10 μM ORF52 protein (3% Alexa 488-labeled) was mixed with 100 ng/μl v-tRNA in 96-well plates coated with 20 mg/ml BSA. Mixtures were incubated and images were captured by confocal microscopy. Bar: 10 μm. **(F)** Phase separation assay of ORF52 with total RNA extracted from infected or uninfected cells was performed in physiological buffer. 10 μM ORF52 protein was mixed with 100 ng/μl total RNA in 96-well plates coated with 20 mg/ml BSA. Mixtures were incubated and images were captured by confocal microscopy. Bar: 10 μm. Source data are available for this figure: SourceData FS2.

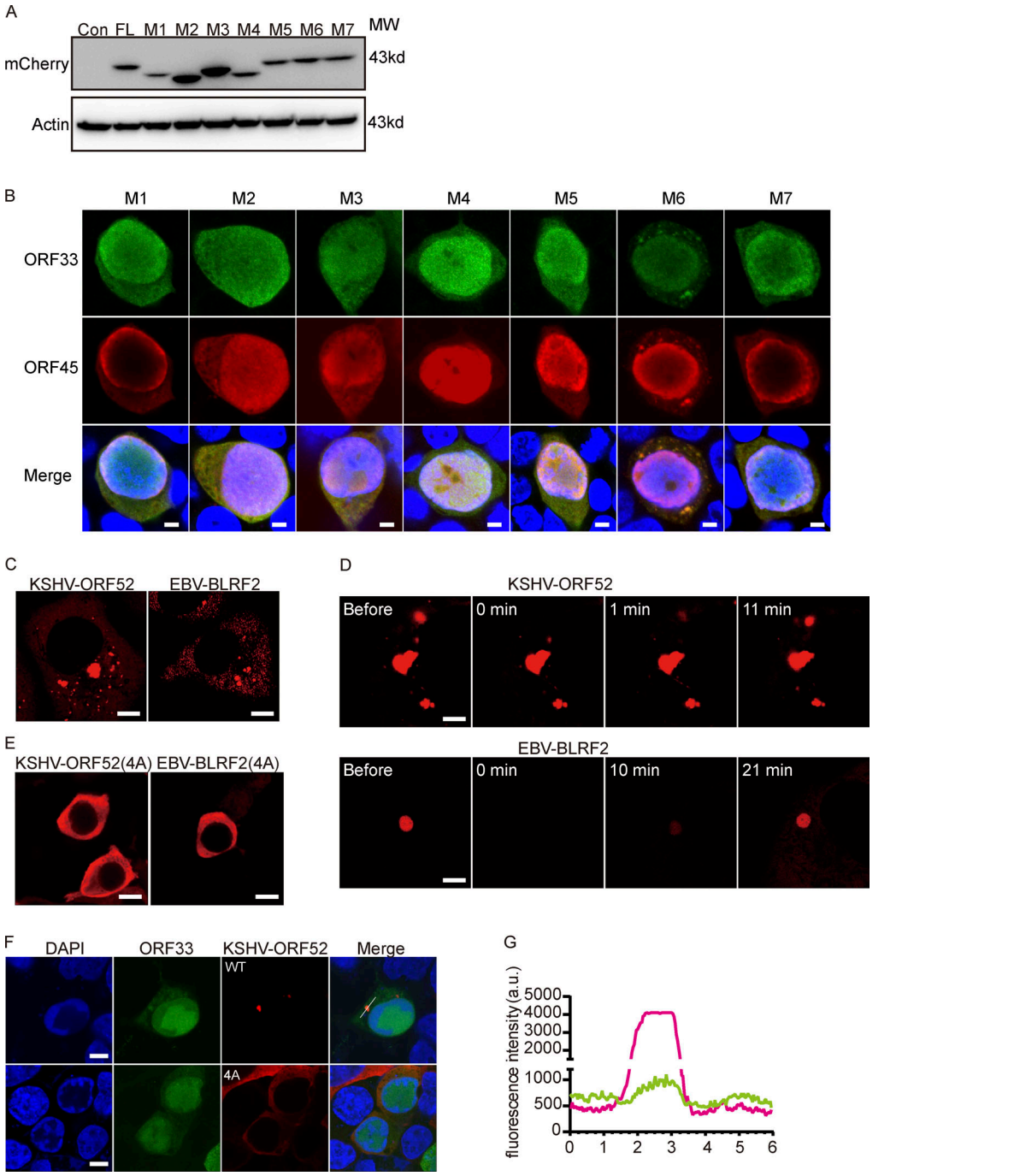

Figure S3. **Analyses of ORF52 mutants and the LLPS properties of ORF52 from other γ-herpesviruses. (A)** Empty vector or plasmids expressing mCherry-ORF52 or plasmids expressing mCherry-tagged mutants were individually transfected into 293T cells. Cells were collected for Western blot at 48 h post transfection. **(B)** 293T cells were transfected with ORF52 mutant BAC and detected by indirect immunofluorescence at 48 h post transfection. ORF33 was detected using a mouse anti-ORF33 monoclonal antibody, followed by an Alexa Fluor 488-conjugated secondary antibody (green channel). ORF45 was detected using a rabbit anti-ORF45 polyclonal antibody, followed by an Alexa Fluor 647-conjugated secondary antibody (red channel). Nuclei were stained with DAPI (blue channel). Bar: 5 µm. **(C)** KSHV-ORF52 and EBV-BLRF2 form puncta in COS-7 cells after transfection. Plasmids expressing mCherry-ORF52 (KSHV) or mCherry-BLRF2 (EBV) were transfected into COS-7 cells. Cells were observed with a fluorescence microscope. Bar: 5 µm. **(D)** FRAP of mCherry-ORF52 homologues in COS-7 cells at 37°C. Bar: 2 µm. **(E)** A conserved cluster of basic amino acids in the IDR is also required for phase separation of KSHV-ORF52 and EBV-BLRF2. Plasmids expressing KSHV mCherry-ORF52(4A) or EBV mCherry-BLRF2(4A) were transfected into COS-7 cells. Cells were observed with a fluorescence microscope. Bar: 10 µm. **(F)** Formation of cVACs relies on the phase separation properties of KSHV ORF52. 293T cells were transfected with MHV-68-ORF52-null BAC plus a plasmid expressing KSHV-ORF52 or its 4A mutant. At 48 h post transfection, MHV-68-ORF33 and KSHV-ORF52 were visualized by indirect immunofluorescence. ORF33 was detected using a mouse anti-ORF33 monoclonal antibody, followed by an Alexa Fluor 488-conjugated secondary antibody (green channel). ORF52 was detected using a rabbit anti-flag monoclonal antibody, followed by an Alexa Fluor 555-conjugated secondary antibody (red channel). Nuclei were labeled with DAPI (blue). Bar: 5 µm. **(G)** Plot of the normalized fluorescence intensity of KSHV-ORF52 (red) and MHV-68-ORF33 (green) along the line in F. Source data are available for this figure: SourceData FS3.

Video 1. **Time-lapse imaging video of cVAC formation.** COS-7 cells were infected with mCherry-ORF52 recombinant virus at a MOI of 3 and images were collected from 12 hpi (00:00:00). cVACs formed gradually in the cytoplasm over time. Data are representative of at least three independent experiments.

Video 2. **Time-lapse imaging video of FRAP of a cVAC in a cell.** COS-7 cells were infected with mCherry-ORF52 recombinant virus at a MOI of 3 and images were collected. Data are representative of at least three independent experiments.

Video 3. **Time-lapse imaging video of FRAP of ORF52 puncta in cells.** FRAP of mCherry-ORF52 in COS-7 cells at 37°C.

Video 4. **Time-lapse imaging video of ORF52-DNA phase separation.** Phase separation of ORF52 with 45-bp ds-DNA was performed in 20 mM Tris-HCl, pH 7.5, 150 mM NaCl. 10 μM ORF52 protein was mixed with 5 μM 45-bp ds-DNA (2% Cy3-labeled) in 96-well plates coated with 20 mg/ml BSA. Mixtures were incubated and images were captured by confocal microscopy.

Video 5. **Time-lapse imaging video of ORF52-RNA phase separation.** Phase separation of ORF52 with total RNA was performed in physiological buffer. 5 μM ORF52 protein was mixed with 100 ng/μl total RNA in 96-well plates coated with 20 mg/ml BSA. Mixtures were incubated and images were captured by confocal microscopy.

Provided online is Table S1. Table S1 shows all nucleic acid sequences used in this work.